

Absorption Spectra of Transition Ions in CdS Crystals

R. PAPPALARDO AND R. E. DIETZ
Bell Telephone Laboratories, Inc., Murray Hill, New Jersey
 (Received March 21, 1961)

The low-temperature optical absorption spectra of single crystals of wurtzite CdS containing impurity ions of the first transition series and one rare-earth ion, ytterbium, were studied in the range of 4.5 to 0.4 μ . The main features of the spectra were found to be in good agreement with a cubic crystal field model, while structure found in the spectral bands of nickel and cobalt impurities could be described by a simple, first-order treatment using the free ion spin-orbit coupling constants. The relevant crystal field parameters, the site symmetry, and formal charges of the impurity ions were determined where possible.

I. INTRODUCTION

MANY properties of impurities in CdS have recently been investigated by such techniques as electron spin resonance,¹⁻³ optical fluorescence,^{4,5} and a variety of photoconductivity effects.⁶ In order to supplement this considerable body of information and also to investigate the limit of applicability of the crystal field theory, we have studied the optical absorption properties of single crystals of CdS doped with ions of the first transition series. In view of the considerable success of the crystal field theory in interpreting analogous properties of aquocomplexes,⁷⁻⁹ oxides,¹⁰⁻¹² and halides,^{13,14} one might expect that the same formalism could be extended to the case of sulfides. According to the crystal field formalism, the $3d$ electrons of the impurity ions are localized on the corresponding ions and are essentially coupled to the lattice by the electrostatic potential of the nearest neighbors. The basic ideas of the crystal field theory are contained in a number of papers¹⁵⁻¹⁸; recent theoretical and experimental work is summarized in the review articles by Fick and Joos¹⁹ and by McClure.²⁰

CdS offers several advantages as a host lattice; paramount among these are the availability of large, pure single crystals having a well-defined structure (wurtzite) and a facile means of introducing impurity ions, namely, by thermal diffusion. There are two disadvantages. The first of these pertains to the very intense edge absorption which commences at approximately 20 000 cm^{-1} , and arises from the excitation of electrons from the valence band to the conduction band of the pure crystal. This absorption obscures the weak absorptions arising from crystal field transitions in that region. The second possible disadvantage arises from the nature of the symmetry of the Cd site. As the CdS crystals studied were of the wurtzite (hexagonal) structure, the sulfide ions do not coordinate the cadmium ions in a regular tetrahedron, but experience a slight uniaxial distortion along the optic axis of the crystal. Three of the sulfide ions forming the tetrahedron lie in a plane normal to the optic axis and are equidistant at 2.53 Å from the central cation. The remaining sulfide ion is extended along the optic axis at a distance of 2.51 Å.²¹ This axial distortion may be expected to produce a small splitting of levels which are degenerate in a perfectly cubic field. As we shall see, this effect complicates the identification of some of the observed fine structure.

We would like to point out that different ionic charges and site symmetries of the same impurity ion should produce drastically different absorption spectra according to the crystal field theory²²⁻²⁴; where positive identification of the spectra of an impurity ion can be accomplished, the determination of ionic charge and site symmetry in CdS will be an important by-product of this investigation.

II. EXPERIMENTAL

A. Preparation of Samples

Single crystals of CdS were obtained from the Eagle Picher Company. These were oriented by polarized

¹ P. B. Dorian, *Phys. Rev.* **112**, 1058 (1958).
² J. Lamb and C. Kikuchi, *Phys. Rev.* **119**, 1256 (1960).
³ J. Lamb, J. Baker, and C. Kikuchi, *Phys. Rev. Letters* **3**, 270 (1959).
⁴ G. Meijer and M. Avinor, *J. Phys. Chem. Solids* **12**, 211 (1960).
⁵ G. Meijer and M. Avinor, *Philips Research Repts.* **15**, 225 (1960).
⁶ R. H. Bube, *Photoconductivity of Solids* (John Wiley & Sons, Inc., New York, 1960).
⁷ C. K. Jorgensen, *Report Xth Solvay Council*, edited by R. Stoops (Brussels, 1956).
⁸ D. G. Holmes and D. S. McClure, *J. Chem. Phys.* **26**, 1686 (1957).
⁹ A. D. Liehr and C. J. Ballhausen, *Phys. Rev.* **106**, 1161 (1957).
¹⁰ M. H. L. Pryce and W. A. Runciman, *Discussions Faraday Soc.* **26**, 34 (1958).
¹¹ W. Low, *Phys. Rev.* **103**, 247 (1958); **109**, 256 (1958).
¹² S. Sugano and Y. Tanabe, *J. Phys. Soc. Japan* **13**, 709 (1959).
¹³ J. W. Stout, *J. Chem. Phys.* **31**, 709 (1959); **33**, 303 (1960).
¹⁴ R. Pappalardo, *J. Chem. Phys.* **31**, 1050 (1959); **33**, 613 (1960).
¹⁵ E. Ilse and H. Hartmann, *Z. physik Chem. (Leipzig)* **197**, 239 (1951).
¹⁶ L. E. Orgel, *J. Chem. Phys.* **23**, 1824 (1955).
¹⁷ Y. Tanabe and S. Sugano, *J. Phys. Soc. Japan* **9**, 753, 766 (1954).
¹⁸ A. D. Liehr, *J. Phys. Chem.* **64**, 43 (1960); also containing an extensive list of references on the subject.
¹⁹ E. Fick and G. Joos, *Handbuch der Physik*, edited by S. Flügge (Springer-Verlag, Berlin, 1957), Vol. 28, p. 205.
²⁰ D. S. McClure, *Solid State Phys.* **9**, 399 (1959).

²¹ R. W. G. Wyckoff, *Crystal Structures* (Interscience Publishers, Inc., New York, 1948), Vol. I, p. 31.
²² C. J. Ballhausen, *Kgl. Danske Videnskab. Selskab, Mat.—fys. Medd.* **29**, No. 4 (1954).
²³ R. Pappalardo, *J. Mol. Spectroscopy* (to be published).
²⁴ R. Pappalardo and D. L. Wood, *J. Chem. Phys.* **33**, 1733 (1960).

TABLE I. Spectrochemical analysis of CdS crystals.

Sample No.	Nominal element doped	(a) Qualitative						
		>10	>1	0.1-3.0	Estimated range (percent)			
					0.01-0.3	<0.03	<0.005	<0.001
<i>I-60-6</i>	Mn	Cd			Mn		Fe	Ag,Al,Ca,Cu, Mg,Si
<i>I-79-2</i>	Cr	Cd			Cr	Mn	Al,Fe,Mg,Si	Ag,Ca,Cu
<i>I-72-3</i>	Cr	Cd				Cr	Fe	Ag,Al,Ca,Cu,Mg, Mn,Si
<i>I-67-5</i>	V,Cu	Cd			Cu,Mn	V	Al,Fe,Mg,Si	Ag,Cu
<i>I-79-3</i>	Cu	Cd			Cu		Fe	Ag,Al,Ca,Mg, Mn,Si
(b) Quantitative								
<i>I-60-6</i>		Mn 0.045%					<i>I-79-3</i>	Cu 0.27%
<i>I-79-2</i>		Cr 0.022%					<i>N-100</i>	Ni 0.018%
<i>I-72-3</i>		Cr 0.0049%					<i>O-100</i>	Co 0.008%
<i>I-67-5</i>		Cu 0.11%; V 0.0053%; Mn 0.023%						

light and cut into slices about a millimeter in thickness such that all faces were either perpendicular or parallel to the optic axis. Films of the various transition metals of a few microns in thickness were evaporated on the surfaces of the slices. The metals were then diffused into the CdS by sealing the crystals in evacuated silica glass tubes and heating in a furnace for several hours. To prevent the crystals from subliming at the high temperatures required for diffusion, small amounts of sulfur were introduced into the capsules. It is possible that by combining with the metal the sulfur also facilitated the introduction of the impurity ions in the crystal. To ensure a maximum concentration of impurities, all samples were quenched by dropping the hot capsules into water.

Of the transition metals, copper and cobalt diffuse most readily into CdS. Although copper diffused rapidly in high concentration (about 0.3%) at 900°C, the most intense spectra were observed when the diffusions were made at 1200°C. Cobalt also has a high rate of diffusion, but has a lower saturation concentration than copper. Diffusion of cobalt at 1150°C was observed to be virtually complete after only 10 or 15 minutes. The saturation concentration of nickel was about the same as for cobalt (about 0.01%), but the rate of diffusion was slower by an order of magnitude. Diffusion of the other transition ions is more difficult, and the saturation concentrations appear to be lower than for copper, cobalt, and nickel. A few microns of the surfaces of most samples were polished off after diffusion; this was particularly necessary for impurities as chromium, vanadium, titanium, and manganese which were relatively insoluble and often remained as visible layers of metal or metal sulfide on the surfaces after diffusion.

The samples containing the intentionally introduced impurities, and the single-crystal CdS starting material were analyzed for impurity content by emission spectrochemical techniques. Table I lists the principal impurities found in the various samples for which spectra

are given in this paper. Samples containing impurity concentrations over a wide range were prepared for each impurity ion. With the exception of chromium, the ratios of the intensities of the various absorption bands, observed for samples containing a given impurity ion, did not vary over the range of concentrations studied. Furthermore, these ratios did not change with the temperature or duration of heating during diffusion. Although we were able to introduce small amounts of Ti into CdS, we did not observe any band spectra for the corresponding ions.

B. Apparatus

A Cary model 14 Universal double-beam spectrophotometer was used in the region 2.6 to 0.2 μ , while for longer wavelengths a single-beam Perkin-Elmer model 112 spectrophotometer was used. At 78°K, a quartz cryostat and a Pyrex glass cryostat were used for wavelengths shorter than 2.4 μ , while a brass cryostat with NaCl windows was employed at longer wavelengths; for work at 4.2°K a double cryostat of Pyrex glass was used.

Polarized light was used to study the absorption at 78°K of some samples of CdS:Co and CdS:Ni having faces containing the *c* axis. Since only slight differences were observed for the two orthogonal directions of polarization of the incident light, we shall limit our considerations in the present study to optical absorption using unpolarized light.

III. CdS:Cu

A. Observed Spectra

We now consider the optical absorptions of the various iron-group ions in order of increasing number of holes in the 3*d* shell. For Cu²⁺ the electronic configuration is (argon) 3*d*⁹; in other words the system is equivalent to one positive charge in the 3*d* shell. The absorp-

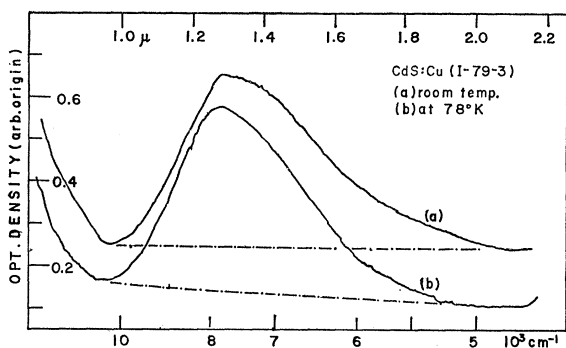


FIG. 1. CdS:Cu sample I-79-3, 0.83 mm thick. Absorption (a) at room temperature; (b) at 78°K.

tion spectra of the various samples of CdS:Cu studied show some differences; we shall discuss in detail the spectra of two representative samples.

Sample I-79-3

Spectrochemical analysis data are given for this sample in Table I. Very little difference is found in the absorption spectra at room temperature and at 78°K: in both cases the absorption is in the form of a rather intense bell-shaped band superposed on a flat background (Fig. 1). The position of the peak (or center) of the band at $\sim 7000 \text{ cm}^{-1}$ found in all Cu-doped crystals is fairly constant.

The oscillator strength was 2×10^{-4} which was calculated by assuming that all the Cu ions present are in the divalent state and occupy tetrahedral sites. Since Cu may also be present in other valence states, the value given for the oscillator strength must be considered as a lower limit of the true value. This value is quite close to the f numbers found²³ for ZnO:Cu. Although the spectrum of this sample is in good agreement with the prediction of the crystal field theory for Cu^{2+} in tetrahedral coordination,²³ a better comparison with the theory can be made by using the spectrum of the following sample, in which structure is present in the absorption at $\sim 7000 \text{ cm}^{-1}$.

Sample A-100

This sample showed at 78°K a considerably narrower absorption in the $\sim 7000 \text{ cm}^{-1}$ region than did the previous sample; also, the edge absorption has been shifted to longer wavelengths. (See Fig. 2.) The band is moderately intense at 78°K and shows some structure. When the sample is cooled to 4.2°K, the intensity of the band is greatly diminished, but the previous (at 78°K) bell-shaped absorption is now resolved into some faint, but reproducible, narrow structure. In effect the absorption consists of a weak but distinct line A at 6430 cm^{-1} which is followed by a poorly resolved doublet B at 6540 cm^{-1} and another at 6800 cm^{-1} . This resolution of the observed spectrum is very similar to the structure

found at 78° and 4.2°K for ZnO:Cu (Fig. 3) and Cu-doped yttrium gallium garnet.²³

B. Energy-Level Scheme for Cu^{2+}

The electronic energy-level scheme (inclusive of spin orbit coupling) for Cu^{2+} in different crystal coordinations has been given by Liehr.¹⁸ In the simple case of cubic symmetry the energy of the three possible levels are given by the following expressions, in which the double-valued representations, for cubic symmetry, of the orbital momentum spin product space²⁵ are used.²⁶

$$\Gamma_7(^2T_2): E = \lambda - 4Dq. \quad (1)$$

$$\Gamma_8: \begin{vmatrix} {}^2T_2 & \\ -\frac{1}{2}\lambda - 4Dq - E & (\frac{3}{2})\lambda \\ (\frac{3}{2})\lambda & 6Dq - E \end{vmatrix} = 0. \quad (2)$$

In this formula λ is the spin-orbit coupling constant and Dq the cubic field parameter, which is the scale factor in the expression for the cubic symmetry potential and is accordingly the only quantity which determines the energy-level ordering in a one-electron system. In terms of physical parameters of the system, $Dq \propto (Z_{\text{eff}}e/R^5)\langle r^4 \rangle$, where Z_{eff} is the effective charge of the nearest neighbors (ligands), $\langle r^4 \rangle$ is the fourth moment of the $3d$ electron, and R the cation-ligand distance. For aquocomplexes of coordination number six, it is found experimentally¹⁶⁻¹⁸ for ions of the first transition series that $Dq \sim 2000 \text{ cm}^{-1}$ for trivalent ions and $Dq \sim 1000 \text{ cm}^{-1}$ for divalent ions. As shown also in Fig. 4, the following relation²² holds for Dq in going from octahedral to tetrahedral coordination of the same

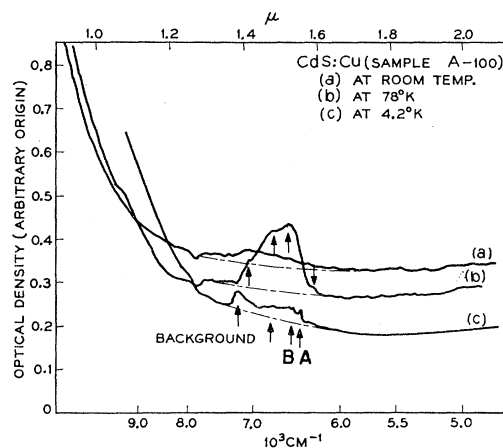


FIG. 2. CdS:Cu sample A-100, 1.46 mm thick. Absorption (a) at room temperature; (b) at 78°K; (c) at 4.2°K. The arrows indicate reproducible fine structure.

²⁵ H. Bethe, Ann. Physik 3, 181 (1929).

²⁶ The following symbols for cubic group representations are equivalent: Γ_1 and A_1 ; Γ_2 and A_2 ; Γ_3 and E ; Γ_4 , T_1 , and F_1 ; Γ_5 , T_2 , and F_2 .

ligands, for cubic site symmetry²⁷:

$$Dq_{tet} = -(4/9)Dq_{oct}. \quad (3)$$

It is also found experimentally that Dq values for coordination six are very similar for both aquocomplexes⁸ and oxides.¹¹ One cannot predict *a priori* what the values of Dq pertaining to a coordination of sulfide ions will be. We expect, though, that the change from Dq (oxides) will not be drastic and from consideration of the relative sizes of the O^{2-} and S^{2-} electronic clouds, we expect that S^{2-} will be located (provided covalency effects are not preponderant) between F^- and O^{2-} in Tsuchida's spectrochemical series,²⁸ which lists the ligands in order of increasing strength of the crystal field as

$$Br < Cl < F < O < N. \quad (4)$$

Figure 4 shows for the case of tetrahedral symmetry the predicted ordering of the energy levels of Cu^{2+} in oxide systems (ZnO, tetrahedral sites of yttrium gallium garnet) and the experimental data for these systems and CdS:Cu. On the basis of the preceding considerations, we may make the following conclusive remarks:

(1). The predictions of the crystal field theory for the energy of electronic transitions within the $3d$ shell of Cu^{2+} in tetrahedral coordination of sulfide ions are in very good agreement with the observed absorption (Figs. 2 and 4).

(2). Departures from cubic symmetry can only cause a twofold splitting of the excited electronic Γ_8 level. The fact that in ZnO:Cu; YGG:Cu, and also CdS:Cu many more lines than the expected maximum of two are observed can be explained on the basis of the Jahn-Teller theorem, as will be shown by Liehr.²⁹

(3). The energy of the observed band does not depend simply on Dq (cubic field parameter) as in the case when the energy levels of Cu^{2+} are treated neglecting spin-orbit effects, but depends also, in a more complete theory, on the value of the spin-orbit coupling

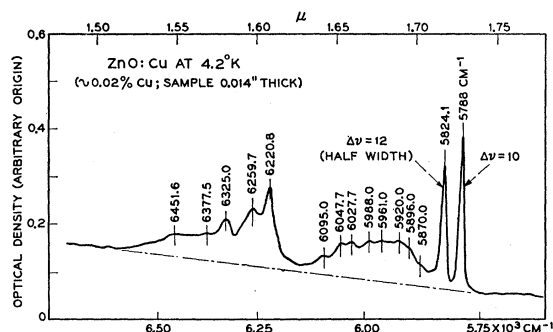


FIG. 3. Absorption spectrum of ZnO:Cu at 4.2°K. (From reference 23.) Compare with Fig. 4.

²⁷ Provided $\langle r^4/R^5 \rangle_{tet} = \langle r^4/R^5 \rangle_{oct}$.

²⁸ R. Tsuchida, Bull. Chem. Soc. Japan **13**, 388, 436, 471 (1938).

²⁹ A. D. Liehr, Progr. Inorg. Chem. (to be published).

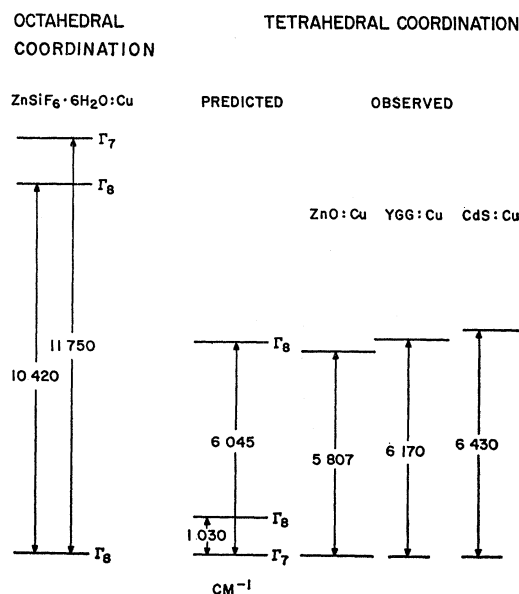


FIG. 4. Predicted and observed energy-level scheme for Cu^{2+} in tetrahedral coordination (from reference 10). YGG stands for yttrium gallium garnet. The energy of the leading absorption line in each system is indicated.

constant λ in the crystal studied. These spin-orbit effects can be considerable: In fact, in the absence of spin-orbit interaction the ground cubic field term 2T_2 is triply degenerate, while in the spin-orbit treatment the $\Gamma_8({}^2T_2)$ multiplet component is increased in energy by some 1000 cm^{-1} , and the excited $\Gamma_8({}^2E)$ is increased by the same amount (Fig. 4).

Thus, although the leading absorption line in CdS:Cu has greater energy than in ZnO:Cu (Fig. 2), it will not be correct to conclude that $Dq(\text{CdS:Cu}) > Dq(\text{ZnO:Cu})$ unless the corresponding values of the spin-orbit coupling constants λ are known in both cases. The frequencies of the impurity absorptions should also differ since the zero-point vibrational energies of the impurity ions are different for the two host lattices.

IV. CdS:Ni

A. Observed Spectra

Similar spectra were observed for the various samples of CdS:Ni studied. The absorption spectra at 4.2°K differ from the spectra taken at 78°K only in the better resolution of the structure of the various absorptions; but no absorptions disappear in cooling from 78° to 4.2°K as was found³⁰ for the corresponding case of ZnO:Ni.

Absorptions found in the 4000 to 4400 cm^{-1} region are only evident at 4.2°K (Fig. 5); another absorption at $\sim 8200\text{ cm}^{-1}$ shows considerable fine structure at 4.2°K (Fig. 6), a rather broad absorption occurs at

³⁰ R. Pappalardo, D. L. Wood, and R. C. Linares, Jr., J. Chem. Phys. (to be published).

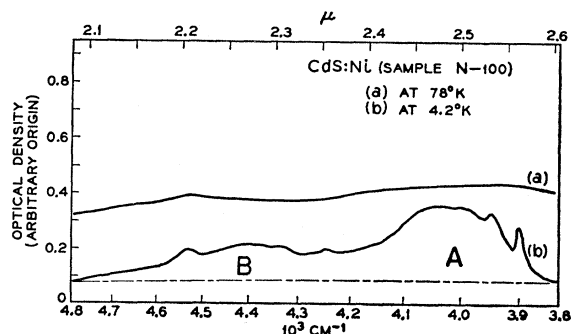


Fig. 5. CdS:Ni sample *N*-100, 1.93 mm thick. Absorption in the 4000 cm^{-1} region: (a) at 78°K; (b) at 4.2°K.

$\sim 10\,000\text{ cm}^{-1}$ (Fig. 6) and there is a very intense band in the $12\,500\text{ cm}^{-1}$ region (Fig. 7). This last absorption is rather broad at room temperature [Fig. 7(a)], but shows a triplet structure at 78°K, while at 4.2°K a more complex pattern appears [Fig. 7(c)]. Finally a narrow, weak absorption appears at $15\,000\text{ cm}^{-1}$ superimposed on the steep slope of the CdS edge absorption (Fig. 8). Oscillator strengths are tabulated for the various absorption bands in Table II.

B. Evaluation of Crystal Field Parameters

While in the one-electron systems the electronic energy scheme (neglecting spin-orbit coupling) depends only on the value of the cubic field parameter Dq , which is a scale factor for the interaction of the $3d$ electron with the rest of the lattice, the energy-level scheme for systems of more than one $3d$ electron must also take into account interactions between the electrons in the $3d$ shell. The additional parameters needed to describe these interactions are Racah's parameters of electrostatic interaction¹⁷ B and C . The general appearance of the absorption spectrum is that of Ni^{2+} in tetrahedral coordination, as can be seen by comparing it, for instance, with the spectrum³⁰ of Ni in ZnO. In the case of CdS, however, a general shift to lower frequencies is observed, as compared with the analogous spectrum in ZnO. Since in the present case the ions coordinated to Ni^{2+} are sulfide ions, this general shift in energy

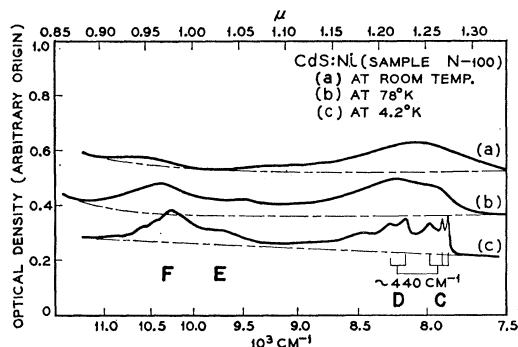


Fig. 6. CdS:Ni sample *N*-100. Absorption in the 7500 cm^{-1} to $11\,000\text{ cm}^{-1}$ region: (a) at room temperature; (b) at 78°K; (c) at 4.2°K.

could be due either to a lower value of the cubic field parameter Dq , or to a considerable decrease in the parameters of electrostatic interaction associated with increased covalency effects, or both.

Six absorption bands have been observed; of these, three are required to determine values for Dq , B , and C from which the energies of the other levels may be predicted. The remaining three observed bands can then be compared with the levels so predicted.

For Ni^{2+} and Co^{2+} and the conjugate $d^2,3$ systems, the positions of the intrasystem (same spin multiplicity) bands are fixed by only the two parameters

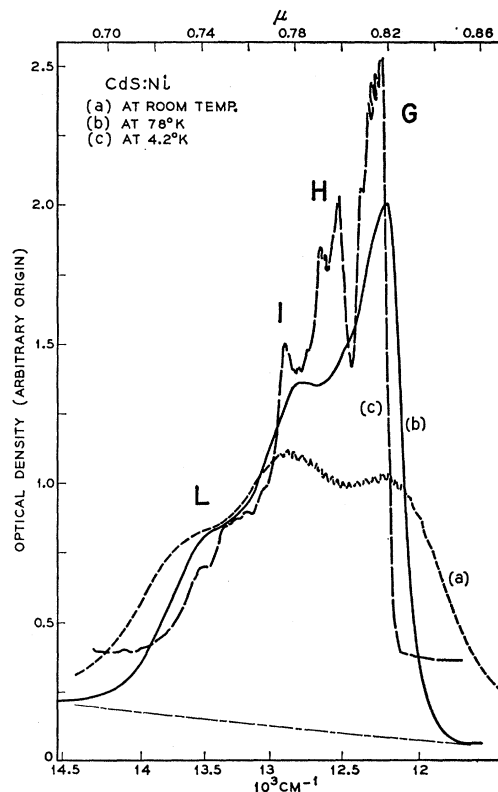


Fig. 7. CdS:Ni sample *N*-100. Intense absorption band in the $13\,000\text{ cm}^{-1}$ region: (a) at room temperature; (b) at 78°K; (c) at 4.2°K.

Dq and B , if spin-orbit coupling effects are neglected. Thus, the observed positions for the two intense bands in Ni^{2+} should determine the value of Dq and B ; for this purpose, we make the following assignments:

Observed absorption	Corresponding electronic transition
$\sim 4000\text{ cm}^{-1}$	${}^3T_1 \rightarrow {}^3T_2$
$\sim 12\,500\text{ cm}^{-1}$	${}^3T_1 \rightarrow {}^3T_1$

To evaluate Dq and B from the observed energies of transitions between multiplet components of cubic field terms, one must calculate the energy difference of the *baricenters* of the corresponding multiplets.

The first assignment (5), which neglects the spin-orbit coupling effects, was used to deduce approximate values of B and Dq ; these values were then used, following the method of reference 30, to evaluate the magnitude of the spin-orbit splitting constants^{30,31} c_a and c_b for the 3T cubic symmetry terms and so provide an estimate of the (first order) spin-orbit splitting both in the ground and excited terms. The quantities c_i are given by:

$$c_b = 2\cos^2\theta + \sin^2\theta + 2\sin 2\theta, \quad (6a)$$

$$c_a = 2\cos^2\theta' + \sin^2\theta' + 2\sin 2\theta', \quad (6b)$$

where

$$\tan 2\theta = \frac{-12B}{10Dq - 9B};$$

$$\sin 2\theta = -12B[225B^2 - 180DqB + 100Dq^2]^{-\frac{1}{2}}, \quad (7a)$$

$$\tan 2\theta' = \frac{-12B}{10Dq - 9B};$$

$$\sin 2\theta' = 12B[225B^2 - 180DqB + 100Dq^2]^{-\frac{1}{2}}, \quad (7b)$$

TABLE II. Oscillator strengths.

Ion	Band	Oscillator strength		
		$\sim 300^\circ\text{K}$	78°K	4.2°K
Cu(I-79-3)		2.6×10^{-4}	2.0×10^{-4}	
Ni(N-100)	AB	9×10^{-5}		2×10^{-4}
	CD	4×10^{-4}	1.7×10^{-4}	1.3×10^{-4}
	EF		3×10^{-4}	3×10^{-4}
	GHIL	3×10^{-3}	3.5×10^{-3}	2.2×10^{-3}
Co(O-100)	H	1.2×10^{-3}	1.36×10^{-3}	2.0×10^{-3}
	D	0.8×10^{-2}	0.9×10^{-2}	0.9×10^{-2}
				0.85×10^{-4}
	G			2×10^{-4}
Mn(I-60-6)			4.5×10^{-4}	1.5×10^{-4}
	A		1.6×10^{-3}	1.5×10^{-3}
	B			
Cr(I-72-3b)				
	A	0.85×10^{-3}	1.5×10^{-3}	
	B		1.7×10^{-3}	
Cr(I-79-2)				
	A			
	B			
V(I-67-5)	A	6.4×10^{-3}	7.0×10^{-3}	8.0×10^{-3}
	B		1.9×10^{-3}	3.3×10^{-3}

and

$$|{}_a^3T_1\rangle = \cos\theta' |{}^3T_1(d\epsilon^4d\gamma^4)\rangle - \sin\theta' |{}^3T_1(d\epsilon^5d\gamma^3)\rangle, \quad (8a)$$

$$|{}_b^3T_1\rangle = \cos\theta |{}^3T_1(d\epsilon^4d\gamma^4)\rangle - \sin\theta |{}^3T_1(d\epsilon^5d\gamma^3)\rangle. \quad (8b)$$

We thus expect the ground term to be stabilized, due to spin-orbit coupling effects, by some 600 cm^{-1} (separation of the baricenter of the ground multiplet from the lowest multiplet component). The position of the baricenter of the 3T_1 multiplet is then assumed to be given by the position of the first intense peak of the band at $\sim 12500 \text{ cm}^{-1}$, plus the quantity $\sim \frac{3}{4}\zeta_d \sim 470 \text{ cm}^{-1}$, which is half the predicted width of the 3T_1 multiplet in first order, minus the ground state stabilization. Analogous procedures apply to 3T_2 .

³¹ S. Koide, Phil. Mag. 4, 243 (1959).

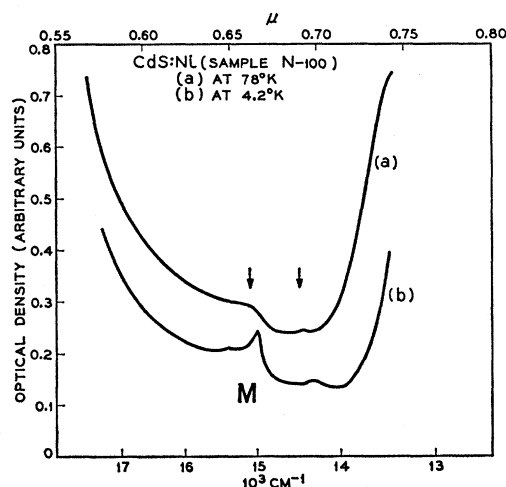


FIG. 8. CdS:Co sample N-100. Weak absorption in 15000 cm^{-1} region: (a) at 78°K ; (b) at 4.2°K .

The remaining levels, as can be easily seen from group theory considerations, are not split by spin-orbit effects in first order, and so, in order to estimate their predicted energy, one needs only be concerned with the ground term spin-orbit stabilization. When this procedure is followed, the values of the Dq and B parameters are obtained as

$$B = 615 \text{ cm}^{-1}, \quad Dq = 415 \text{ cm}^{-1}. \quad (9)$$

It is interesting to remark that while B is considerably smaller, Dq is not very different from the value found³⁰ for ZnO:Ni, namely $B = 795 \text{ cm}^{-1}$ and $Dq = 405 \text{ cm}^{-1}$. A decrease in the values of the parameters of electrostatic interaction points to a larger degree of covalency.

Morin³² and Liehr and Ballhausen³³ have recently discussed the effect of strong covalency on the value of the cubic field parameter Dq , which should now be understood as characterizing the energy differences between molecular orbitals of e and t_2 symmetry. When treating the one-electron problem in a system in which the energy-level scheme is as depicted in Fig. 9, an

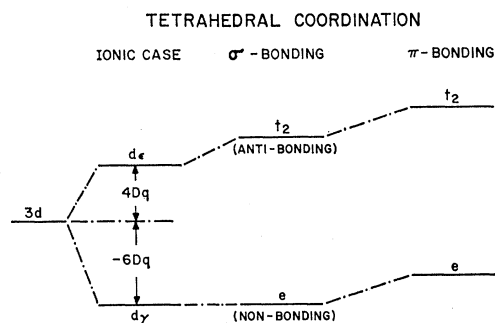


FIG. 9. Effect of covalency on magnitude of Dq .

³² F. Morin, Proceedings of the International Conference on Semiconductors (Prague, 1960).

³³ A. D. Liehr and C. J. Ballhausen, J. Mol. Spectroscopy 2, 342 (1958); 4, 190(E) (1960).

increase in covalency tends to increase the energy of the antibonding t_2 orbitals with respect to the non- σ -bonding e orbitals. Therefore, covalency will cause an increase in Dq , when compared to the limiting case of a purely ionic system, to the point where π bonding causes a destabilization of the e non- σ -bonding orbitals by making them π antibonding and the two processes start competing.

On the other hand, from a comparison of the ionic radii (Ahrens³⁴ gives 0.97 Å for Cd²⁺ and 0.74 Å for Zn²⁺), lower values of Dq and B would be expected for impurity ions in CdS than for the same ions in ZnO, in the absence of covalency effects and lattice distortion at impurity ion sites.

Using the values of B and Dq of Eq. (9), one can calculate the values of the constants for the spin-orbit splitting of the 3T_1 manifolds:

$$c_a = 2.907, \quad c_b = -1.906,$$

and the form of the wave functions:

$$\begin{aligned} |{}_a^3T_1\rangle &= 0.9474 |d\epsilon^4d\gamma^4\rangle - 0.3203 |d\epsilon^5d\gamma^3\rangle, \\ |{}_b^3T_1\rangle &= +0.3203 |d\epsilon^4d\gamma^4\rangle + 0.9474 |d\epsilon^5d\gamma^3\rangle. \end{aligned} \quad (10)$$

From these data the position of the remaining triplet level ${}^3A_2 |d\epsilon^6d\gamma^2\rangle$ is predicted at 8285 cm⁻¹. Experimentally, a band is found centered at ~ 8000 cm⁻¹ (Fig. 6).

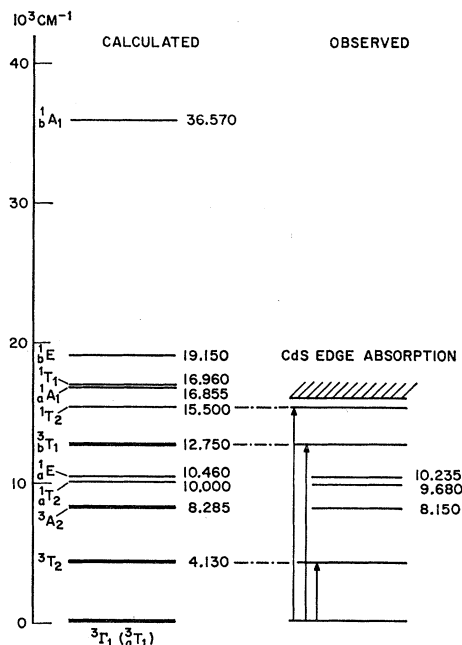


FIG. 10. Energy-level scheme for CdS:Ni. Left: Calculated assuming divalent nickel in tetrahedral coordination with $B=615$ cm⁻¹, $C=4.38$ B, $Dq=415$ cm⁻¹, and spin-orbit stabilization of the ground state as 600 cm⁻¹. Right: Observed absorptions. The energy separations indicated by arrows were used to calculate the energy levels on the left.

³⁴ L. H. Ahrens, Geochim et Cosmochim Acta 2, 155 (1952).

C. Position of the Singlet Levels

From the Tanabe and Sugano¹⁷ energy-level scheme no singlet levels are expected at energies lower than that of 3T_1 . In the observed absorption spectrum, a weak absorption, slightly affected by temperature changes, is found at ~ 15000 cm⁻¹. We shall assume that it corresponds to the ${}^3T_1 \rightarrow {}^1T_2$ transition. Using the values of Dq and B of Eq. (9), we then calculate $C=2695$ cm⁻¹, which implies $C/B=4.4$, close to the value 4.709 found for the Ni²⁺ free ion.

We are now able to predict what the complete energy-level scheme should be for Ni²⁺ in CdS. This is shown in Fig. 10.

D. Spin-Orbit Coupling Effects (First Order)

Only the triplet cubic field terms 3T_1 and 3T_2 will be split by spin-orbit coupling, while the remaining triplets 3A_2 will remain unsplit. This can be easily seen by considering the following products of the representations corresponding to the spin and orbital angular

TABLE III. First-order spin-orbit splitting of 3T cubic field terms.

3T_2 :	$W_1 = \frac{1}{2}\zeta d$	(Symmetry properties: Γ_2)
	$W_2 = \frac{1}{4}\zeta d$	(Symmetry properties: Γ_5)
	$W_3 = -\frac{1}{4}\zeta d$	(Symmetry properties: Γ_3, Γ_4)
3T_1 : ($i=a, b$)	$W_1 = \frac{1}{4}\zeta d c_i$	(Symmetry properties: Γ_3, Γ_4)
	$W_2 = -\frac{1}{4}\zeta d c_i$	(Symmetry properties: Γ_3, Γ_5)
	$W_3 = -\frac{1}{2}\zeta d c_i$	(Symmetry properties: Γ_1)

momentum:

$$\Gamma_4 \times \Gamma_1 = \Gamma_4, \quad (11a)$$

$$\Gamma_4 \times \Gamma_2 = \Gamma_5, \quad (11b)$$

$$\Gamma_4 \times \Gamma_4 = \Gamma_1 + \Gamma_3 + \Gamma_4 + \Gamma_5, \quad (11c)$$

$$\Gamma_4 \times \Gamma_5 = \Gamma_2 + \Gamma_3 + \Gamma_4 + \Gamma_5, \quad (11d)$$

since $S=1$ transforms as Γ_4 .

The product corresponding to 3A_2 contains only one cubic field representation in the total angular momentum space; similar considerations apply to all the singlet terms. Shifting of the position of 3A_2 and of the singlet terms may occur only when matrix elements of spin orbit connecting different cubic field terms are taken into account. The effect of the spin-orbit coupling on 3T_1 and 3T_2 is quite similar³⁰ to the effect in MgO:Ni and ZnO:Ni.

Group theory can be used to predict the maximum number of multiplet components which arise from the 3T manifolds [Eqs. (11)], while the actual detail of the spin-orbit interaction may be obtained by using the Tanabe and Kamimura formalism³⁵; details of the calculation are given in the similar paper³⁰ on Ni²⁺ in

³⁵ Y. Tanabe and H. Kamimura, J. Phys. Soc. Japan 13, 394 (1958).

cubic symmetry, and the results of the calculation are listed in Table III.

Term 3T_1 . The lowest component of the ground multiplet should be, according to Table III, a Γ_1 level, followed by a triply degenerate and a fivefold degenerate multiplet component (Table III). The energy spacings are $\frac{1}{4}\zeta c_a$ and $\frac{1}{2}\zeta c_a$ respectively; the over-all width of the multiplet is $\frac{3}{4}\zeta c_a \sim 470 \times 2.9 = 1360 \text{ cm}^{-1}$, assuming for ζ the approximate value ${}^7 630 \text{ cm}^{-1}$.

Term 3T_2 . The ordering of the multiplet components will be inverted and the spacing will be different, since $c_b = -1.906$.

Term 3T_2 . The multiplet component lowest in energy should be fivefold degenerate, followed by a threefold degenerate level $\frac{1}{2}\zeta \sim 315 \text{ cm}^{-1}$ distant and this by a nondegenerate level spaced $\frac{1}{4}\zeta \sim 157.5 \text{ cm}^{-1}$ further away.

The predicted splitting pattern and the observed energy spacings are collected in Fig. 11. While the previous spin-orbit splitting is limited to a first-order treatment, Liehr and Ballhausen³⁶ have treated the effect of spin-orbit coupling on Ni^{2+} and V^{3+} simultaneously with Coulombic interaction and cubic field effects, and plotted as a function of Dq using the exemplary set of parameters $B = 810 \text{ cm}^{-1}$, $C = 3.9 B$, the energy levels obtained from the computer solution of a number of secular equations. For CdS:Ni , B is quite different from the B values used by Liehr and Ballhausen so that a direct comparison of CdS:Ni spectra with the calculations of these authors can only give an indication of the magnitude of second-order effects of spin-orbit coupling in CdS:Ni .

E. Comparison with Experiment

The preceding discussion of the electronic energy-level scheme has been based on the hypothesis of a predominant cubic field and on the first order treatment of the spin-orbit coupling. The predictions of this model will now be compared with the observed spectra ignoring noncubic components of the crystalline potential, higher order effects of spin-orbit coupling, and the contribution of vibrations to the process of optical absorption.

Ground Term 3T_1 . In considering the intensity pattern of the absorption located at $\sim 12\,500 \text{ cm}^{-1}$ as it appears at room temperature, 78° and 4.2°K , it seems that a contribution exists at room temperature from a state $\sim 500 \text{ cm}^{-1}$ above the ground state (Fig. 7). This is in agreement with the predicted spin-orbit splitting of the ground cubic field term (Fig. 11). Apart from this, there is no contribution from a level of the ground manifold at about 150 cm^{-1} above the lowest state, as was found in ZnO:Ni .

Term 3T_2 . This corresponding absorption can be roughly considered as made up of two groups, separated by some 400 cm^{-1} (Fig. 5). The first group shows four

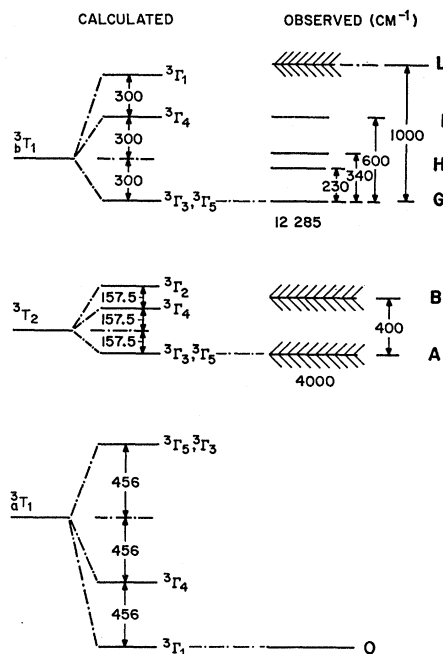


Fig. 11. CdS:Ni . Left: Predicted first order spin-orbit splitting assuming $\lambda = 630 \text{ cm}^{-1}$; $Dq = 415 \text{ cm}^{-1}$; $B = 615 \text{ cm}^{-1}$. Right: Observed energy separation of fine structure. The term separations ${}^3T_1 \rightarrow {}^3T_2$; ${}^3T_1 \rightarrow {}^3T_2$ are not drawn to scale.

peaks, which may possibly arise from the lifting of the cubic field degeneracy of 3T_5 and 3T_3 ,³⁷ while the four peaks of the second group may be associated with 3T_4 and 3T_2 (Fig. 11). So far, the simplified model used seems to be able to predict the main features of the fine structure of the absorption spectrum.

Term ${}^3A_2(d\epsilon^6d\gamma^2)$. This simple model is inadequate, however, to interpret the complex pattern at $\sim 8000 \text{ cm}^{-1}$; according to our predictions the transition should be to 3A_2 . The intensity of this group is considerably lower than that corresponding to the transition to the other triplet at $12\,500 \text{ cm}^{-1}$, but this is reasonable since the ground term has essentially the configuration $d\epsilon^4d\gamma^4$ [Eq. (10)] so that the transition to 3A_2 involves a change of two electrons in the subshell configurations, and is therefore a transition of low probability.

As for the number of fine-structure components in the absorption, if our assignment is correct one would expect no more than three lines, even if low-symmetry components of the field cause a splitting of the multiplet component Γ_5 [Eq. (11b)]. However, in Fig. 6, the sharp triplet C seems to be followed by a vibrational replica D , located 440 cm^{-1} away, which is, incidentally, similar to the separation of the two observed groups A and B belonging to 3T_2 .

Term 1T_2 and 1E On the basis of the spectra of aquo-complexes³⁸ and oxides,^{10,12} absorptions corresponding

³⁷ The Γ_i notation specifies the over-all spin orbit state symmetry, while the superscript designates the predominant spin multiplicity contribution to a given spin orbital state.

³⁸ R. Pappalardo, Phil. Mag. **9**, 1397 (1958); **4**, 219 (1959).

³⁶ A. D. Liehr and C. J. Ballhausen, Ann. Phys. (N.Y.) **6**, 134 (1959).

to transitions to the singlet terms, which have essentially the same subshell configuration as the ground term, should be narrower than observed experimentally in CdS:Ni at 4.2°K in the 10 000 cm^{-1} region. In the present case, however, Dq is smaller and so Coulomb mixing of $a^1\Gamma$ and $b^1\Gamma$ ($\Gamma=A_1, E, T_2, T_1$) terms is more important than in aquocomplexes and oxides and could partly account for the observed broadening as could spin-orbit mixing of singlet and triplet terms. However, the positions of the centers of the two bands correspond rather well to the predicted energy levels, as shown in Fig. 10.

Term b^3T_1 . The observed pattern at $\sim 12\,500\text{ cm}^{-1}$ seems in fair agreement with the simple model based on cubic symmetry potential and spin-orbit coupling. The decrease in the intensity with increasing frequency can be correlated in this context to the predicted decrease in the cubic symmetry degeneracy of the multiplet component in going to higher energies (Fig. 11). From Fig. 7, it is seen that the structure of the band at 78°K can be explained by first-order spin-orbit coupling without invoking lattice vibration contributions to the absorption. The new peaks present in the 4.2°K spectrum may be associated with the lifting of the degeneracy of the cubic field multiplet components $^3\Gamma_3$ and $^3\Gamma_5$. On the other hand, the second peak found at 4.2°K, which is $\sim 350\text{ cm}^{-1}$ away from the most intense absorption, could be a vibrational replica of the first one, since it involves an energy difference already found in other regions of the spectrum. The latter hypothesis can be investigated only by a systematic comparison with the absorption spectrum of other ions in CdS.

F. Concluding Remarks

There is a very satisfactory agreement between the predicted position of the first six excited terms of Ni^{2+} in CdS and the corresponding absorption bands. As a further indication of the reliability of the crystal field approach, the value $Dq(\text{CdS:Ni})=415\text{ cm}^{-1}$, derived from the absorptions taking into account the spin-orbit stabilization, is in good agreement with the value one would expect for Dq in tetrahedral symmetry. Rather surprising is the low value of the B parameter: the hypothesis has been advanced that both the decrease in B and the slight increase of Dq in going from ZnO to CdS are an indication of stronger covalency effects in CdS.

A second point concerns the interpretation of the fine structure. The simple model we have used, namely consideration only of first-order spin-orbit effects, neglecting vibrational contributions and the effect of low-symmetry components of the potential, provides a satisfactory explanation of the structure observed in the individual absorption bands. But a more detailed agreement of theory and experiment for the fine structure is only sporadic.

V. CdS:Co

A. Observed Spectra

Several samples of CdS:Co were studied, all showing identical spectra; we discuss here in detail sample O-100.

The absorption spectrum in the 2.6- to 0.4- μ region was taken at room temperature, liquid nitrogen and liquid helium temperature, using the Cary 14 Universal spectrophotometer. Figures 12 and 13 and Table II give the details of the observed absorptions. Two intense absorptions are found one in the $\sim 6000\text{ cm}^{-1}$ region (band H) and another at $14\,000\text{ cm}^{-1}$ (band D). A much weaker absorption (G) is also present at $\sim 16\,400\text{ cm}^{-1}$. The spectrum was also investigated in the region 4.2 to 2.0 μ using a Perkin-Elmer model 112 spectrometer. No absorptions were observed in this region, however, either at room temperature or at 78°C.

The effect of cooling at 78°K on the band D is to resolve the broad band, which has very little structure at room temperature, into a set of three similar line groups (H_1, H_2, H_3). The fine structure of each of these groups is much more distinct at 4.2°K, and the leading lines of each group shows enhanced intensity [Fig. 12(c)].

The intense band D at room temperature shows a peak at $13\,477\text{ cm}^{-1}$ and an indication of a double structure at $14\,500\text{ cm}^{-1}$. By cooling to 78°K, a pattern of four narrow bands (D_1, D_2, D_3 , and D_4), progressively decreasing in intensity, becomes evident. No remarkable changes in the absorption are brought about by lowering the temperature to 4.2°K. It is interesting that much of the low-energy tail present in the absorption band D at room temperature disappears at 78° and 4.2°K (Fig. 13).

B. Identification of Absorption Bands

As with nickel and copper, we shall compare the observed spectra with that predicted for Co^{2+} sites possessing tetrahedral symmetry.

The energy-level scheme for the quartet terms of the configuration $3d^7$ depends only on the value of two quantities, B and Dq . Since the values of these parameters should be similar for Co^{2+} in either CdS or ZnO, we can make the following assignments by referring to the spectra³⁹ observed for ZnO:Co (recall the related dis-

TABLE IV. Values of crystal field parameters obtained from optical absorption.

	MgO ^a	ZnO ^a	CdS
$ Dq $ (cm^{-1})	927	390	316
B (cm^{-1})	845	700	664

^a See reference 39.

³⁹ R. Pappalardo, D. L. Wood, and R. C. Linares, Jr. (to be published).

cussion of Sec. IV for the analogous nickel systems):

Absorption band	Transition
$\sim 6000 \text{ cm}^{-1}$	${}^4A_2 \rightarrow {}^4T_1$
$\sim 15\,000 \text{ cm}^{-1}$	${}^4A_2 \rightarrow {}^4T_1$

(12)

A more accurate evaluation of the position of the cubic field terms should take into account possible splittings of the terms due to spin-orbit coupling and noncubic components of the field. Since for Co^{2+} the spin-orbit coupling constant has a high value ($\zeta_d = 540 \text{ cm}^{-1}$ for the free ion in the nlm_1m_s scheme) one expects considerable spin-orbit splitting of the excited 4T_1 , 6T_1 , and 4T_2 cubic symmetry terms, while the ground state 4A_2 will be unsplit and unshifted in first order.

From the treatment³⁹ of $\text{ZnO}:\text{Co}$ one expects in the present case an upper limit of 600 cm^{-1} for the total multiplet width of 6T_1 . As for the determination of the baricenter of the 4T_2 term, we can take as a good approximation the center of the triplet structure of band H .

The following assignments are then made for the positions of the baricenter of the cubic field terms:

$${}^4A_2 \rightarrow {}^4T_1 = 550 \text{ cm}^{-1} \text{ (center of band } H\text{)};$$

$${}^4A_2 \rightarrow {}^6T_1 = 13\,950 \text{ cm}^{-1} \text{ (first intense peak of band } D\text{, plus half the predicted multiplet width).} \quad (13)$$

By using the energy matrix elements given by Tanabe and Sugano,¹⁷ one can derive from (13) the following values of the parameters:

$$Dq = 316 \text{ cm}^{-1}, \quad B = 664 \text{ cm}^{-1}. \quad (14)$$

In Table IV, we collect the results of similar calculations based on the study of Co^{2+} in different host lattices.

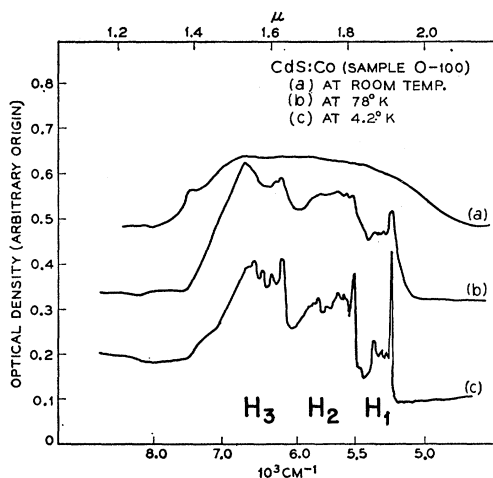


FIG. 12. $\text{CdS}:\text{Co}$ sample O-100, 1.38 mm thick. Absorption in 6000 cm^{-1} region: (a) at room temperature; (b) at 78°K ; (c) at 4.2°K . Note the very sharp peak (half-width: 6.5 cm^{-1}) at the beginning of absorption at 4.2°K .

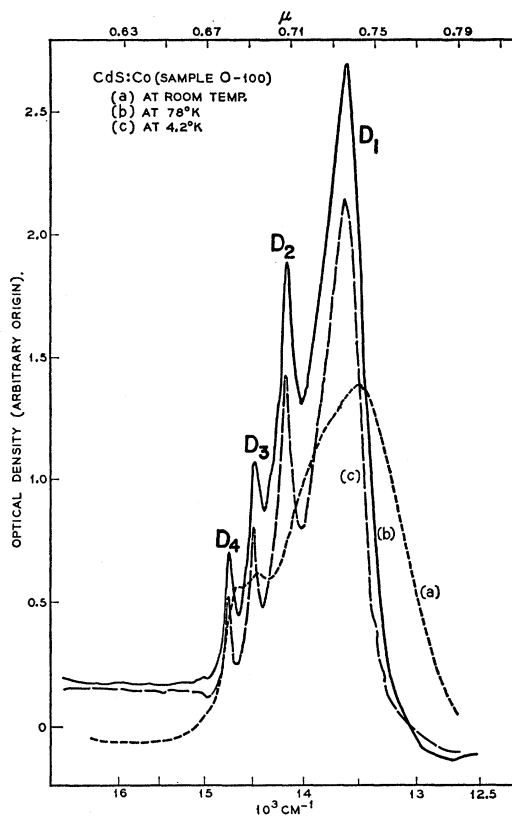


FIG. 13. $\text{CdS}:\text{Co}$ sample O-100. Intense absorption band in visible region: (a) at room temperature; (b) at 78°K ; (c) at 4.2°K . Compare structure of absorption to that of Fig. 9 ($\text{CdS}:\text{Ni}$).

The wave functions of the 4T_1 terms are also given for the evaluation of spin-orbit coupling effects:

$${}^6T_1 = 0.8163 |d\epsilon^4 d\gamma^3\rangle + 0.5776 |d\epsilon^5 d\gamma^2\rangle,$$

$${}^4T_1 = -0.5776 |d\epsilon^4 d\gamma^3\rangle + 0.8163 |d\epsilon^5 d\gamma^2\rangle. \quad (15)$$

The complete energy level scheme for the configuration $3d^7$ can be calculated when the value of the parameter C of electrostatic interaction is known: A typical value is $C = 4.5 B$. The energy level diagram for $\text{CdS}:\text{Co}$ is then obtained after solving the relative secular equations and is shown in Fig. 14. In the Appendix we tabulate the wavefunctions for the doublet levels as linear combinations of states having a definite subshell configuration and symmetry classification. This form for the wavefunction is useful in the treatment of spin-orbit coupling by means of the Tanabe and Kamimura formalism.³⁵

C. Spin-Orbit Coupling Effects

When the effect of the spin-orbit coupling is treated in first order, using as basis the cubic field d -functions, only the spin-orbit interaction within the individual cubic field terms need be considered; the spin orbit mixing of different terms may be neglected. The first-

TABLE V. Double-valued representations in spin-angular momentum product space.

4T_1 :	$\Gamma_8 \times \Gamma_4 = \Gamma_6 + \Gamma_7 + 2\Gamma_8$
4T_2 :	$\Gamma_8 \times \Gamma_5 = \Gamma_6 + \Gamma_7 + 2\Gamma_8$
4A_2 :	$\Gamma_8 \times \Gamma_2 = \Gamma_8$
2E :	$\Gamma_6 \times \Gamma_3 = \Gamma_8$
2T_1 :	$\Gamma_6 \times \Gamma_4 = \Gamma_6 + \Gamma_8$
2T_2 :	$\Gamma_6 \times \Gamma_5 = \Gamma_8 + \Gamma_7$
	$[S = \frac{3}{2} \rightarrow \Gamma_8]$
	$[S = \frac{1}{2} \rightarrow \Gamma_6]$

order effects in Co^{2+} can thus be easily calculated by use of the Tanabe and Kamimura formalism.

An indication of the kind of splitting to be expected can be gained from simple group theory by considering the products of representations¹¹ of Table V.

The resulting spin-orbit energy level pattern is given in Table VI.

The values of the spin-orbit splitting constants c_i ($i = a, b$) are derived^{31,39} from the following relations:

$$c_b = \cos^2\theta - 2\sin^2\theta - 2\sin 2\theta, \quad (16)$$

$$c_a = \cos^2\theta' - 2\sin^2\theta' - 2\sin 2\theta', \quad (17)$$

$$\tan 2\theta = -12B/(10Dq + 9B),$$

$$\sin 2\theta = -12B(225B^2 + 180BDq + 100Dq^2)^{-\frac{1}{2}}, \quad (18)$$

$$\theta' = \theta - 90^\circ. \quad (19)$$

Using the values of Dq and B derived above and the wave functions of Eq. (15), the following values of the c_i constants were obtained:

$$c_a = -2.885; \quad c_b = 1.885. \quad (20)$$

The assignment of the symmetry properties of the twofold levels of 4T_1 was done on the basis of the second-order treatment³⁹ of the spin-orbit coupling of 4T_1 and 2T_1 .

Figure 15 shows the predicted multiplet splittings of the cubic field terms and how they compare with the structure of the absorption bands. The amounts of the predicted splittings indicated must be taken as upper limits since they were derived by assuming for the ζ_d constant the same value it has in the free ion (540 cm^{-1}), while a decrease in this value is to be expected if there is considerable overlap with the electronic cloud of the nearest neighbors.

The agreement found for the ${}^a{}^4T_1$ term is quite good; less so for the ${}^b{}^4T_1$ term, but in this region the term

TABLE VI. Spin-orbit splitting (first order) of cubic symmetry quartet terms.^a

4T_2 :	$W_1 = -\frac{1}{4}\zeta_d$	(sixfold; $\Gamma_8 + \Gamma_6$)
	$W_2 = \frac{1}{6}\zeta_d$	(fourfold; Γ_8)
	$W_3 = (5/12)\zeta_d$	(twofold; Γ_7)
4T_1 :	$W_1 = -\frac{1}{4}\zeta_d c_i$	(sixfold; $\Gamma_8 + \Gamma_7$)
	$W_2 = \frac{1}{6}\zeta_d c_i$	(fourfold; Γ_8)
	$W_3 = (5/12)\zeta_d c_i$	(twofold; Γ_6)

^a c_i ($i = a, b$) is the splitting constant for the 4T_1 terms.

${}^b{}^4T_1$ is not well isolated and strong spin-orbit mixing might occur with the doublet terms.

The oscillator strengths are quite high, of the order of 10^{-3} for band H and 10^{-2} for band D . This is in good agreement with the oscillator strengths found³⁹ for ZnO:Co , and with the predicted oscillator strengths³³ for tetrahedrally coordinated Co^{2+} . Transitions corresponding to the lowest excited term 4T_2 were not observed.

Because of the intensity of the Co absorption in the visible region ($\alpha_{\text{max}} \sim 2$ in optical density units) and the characteristic nature of its quartet pattern, it is possible that with a sample 2 or 3 mm thick one can detect 1 part per million of Co^{2+} ions by studying the optical absorption at 78°K .

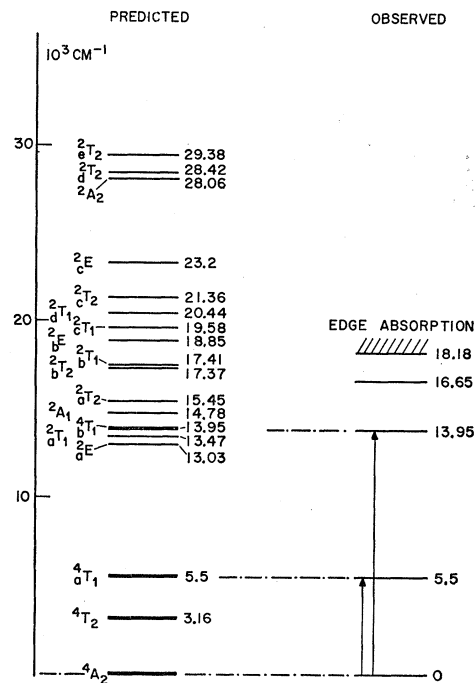


Fig. 14. Energy level scheme for CdS:Co . Left: Predicted energy level scheme (neglecting spin orbit effects) for divalent cobalt in tetrahedral sites with $Dq = 316 \text{ cm}^{-1}$; $Dq = 664 \text{ cm}^{-1}$; $C = 4.5 B$. Right: Experimental absorptions. Energy of levels connected to ground state by arrows were used to derive values for B and Dq .

VI. CdS:Fe

Similar spectra were obtained for the various samples of CdS doped with Fe . Details are reported here for a typical sample, $I-59-i$. The spectrum of this sample (Fig. 16) was studied in the range 4.2 to 0.5μ with the Perkin-Elmer model 112 spectrometer. A single intense band was observed centered about 3.5μ (2860 cm^{-1}). At room temperature the band was fairly broad and featureless, but upon cooling the crystal to 78°K , the absorption was considerably enhanced and several peaks were resolved.

This absorption is compatible with Fe^{2+} in tetrahedral

coordination. Only one intense intrasystem transition is expected for $3d^4$ (and the conjugate $3d^6$ system); in ferrous aquocomplexes this transition is observed⁸ as a broad band at $10\,000\text{ cm}^{-1}$, with an oscillator strength of 0.4×10^{-4} . For Fe^{2+} in tetrahedral coordination this intense band should occur at

$${}^5E \rightarrow {}^5T_2 = 10Dq, \quad (21)$$

neglecting effects of spin-orbit coupling. Now

$$|(4/9)Dq[\text{Fe}(\text{H}_2\text{O})_6^{3+}]| = 450\text{ cm}^{-1}, \quad (22)$$

so, in view of the decrease of the value of Dq in going from coordination of water to the coordination of sulfide

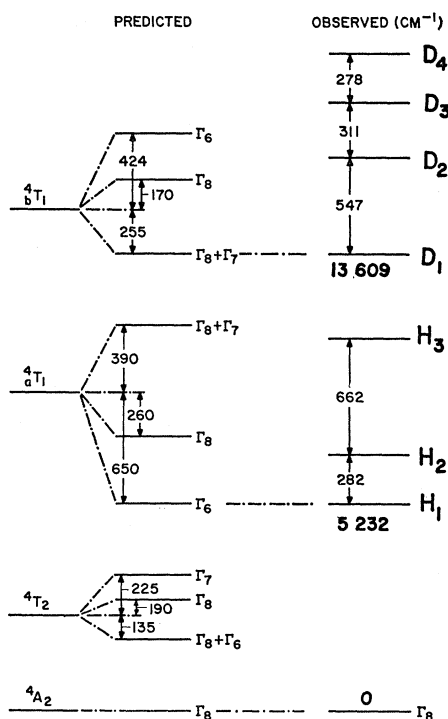


FIG. 15. CdS:Co. First-order treatment of spin-orbit effects on 4T_1 , 6T_1 , and 4T_2 terms. Left: Calculated splitting ($\lambda=540\text{ cm}^{-1}$; $c_a=-2.885$; $c_b=1.885$). Right: Observed structure in the bands at $\sim 5500\text{ cm}^{-1}$ and $\sim 14\,000\text{ cm}^{-1}$. The splittings are drawn to scale, while the separations of the cubic field terms from the ground term 4A_2 are not.

ions in CdS, one would expect an intense band centered around $\sim 3800\text{ cm}^{-1}$, which is in poor agreement with the center of the observed band. It is possible that by considering the effect of spin-orbit stabilization of the ground state on the position of the observed bands, the predicted and observed values of Dq might be brought into closer agreement, but we do not expect this effect to account for a substantial part of the discrepancy. On the other hand the energies associated with Jahn-Teller distortions of the ground and excited terms can be large (about 500 cm^{-1} for the ground state⁴⁰ of VCl_4) and could possibly be responsible for the discrepancy.

⁴⁰ C. Ballhausen and A. D. Liehr, Acta. Chem. Scand. (to be published).

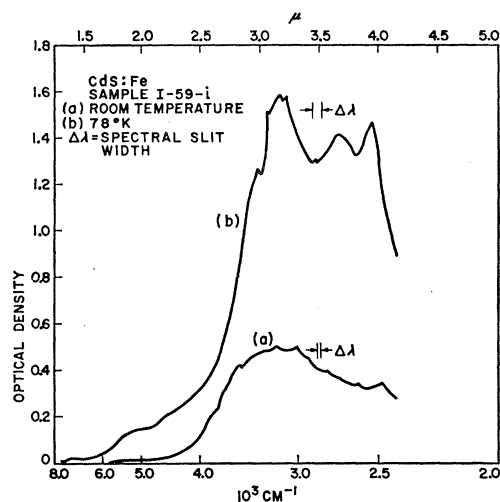


FIG. 16. CdS:Fe sample *I-59-i*, 0.63 mm thick. This intense band, centered about 3000 cm^{-1} is the only absorption observed.

VII. CdS:Mn

Since similar spectra were observed for all of the CdS:Mn samples studied, we shall discuss in detail the spectrum of a typical sample, *I-60-6*, which was also analyzed spectrochemically for impurity content (Table II). Only one absorption band is found (Fig. 17); at 78°K a band stretches from 1.58 to $1.04\ \mu$ (6630 cm^{-1} to 9615 cm^{-1}) peaking at $1.3\ \mu$ (7690 cm^{-1}), over a background continuous absorption starting at $2.2\ \mu$ and coalescing with the CdS edge absorption. The oscillator strength of the band at $1.3\ \mu$ is calculated as 2.0×10^{-4} , assuming all Mn ions are equivalent with respect to ionic charge and site symmetry; since these two assumptions may not be valid, the value given for the oscillator strength must be considered a lower limit. The edge absorption reaches optical density unity over the extrapolated background at $6300\ \text{\AA}$ ($15\,870\text{ cm}^{-1}$).

At 4.2°K no remarkable changes in the shape of the band or in its intensity are found: the band now shows a double structure with peaks at $1.28\ \mu$ (7812 cm^{-1})

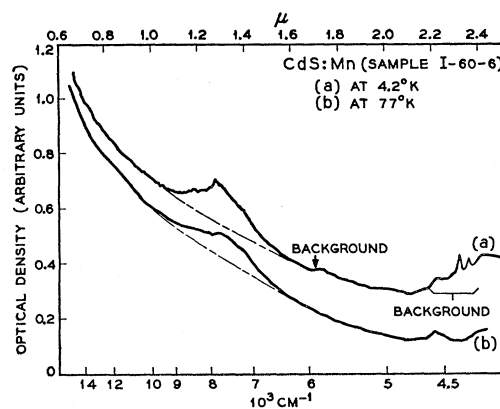


FIG. 17. CdS:Mn sample *I-60-6*, 1.16 mm thick. Absorption band at $\sim 8000\text{ cm}^{-1}$: (a) at 4.2°K ; (b) at 78°K .

and 1.18μ (8475 cm^{-1}). The oscillator strength is 1.8×10^{-4} . The optical density of the edge absorption is *unity* at 6100 \AA (16390 cm^{-1}). The most probable valence states for Mn ions in CdS are Mn^{2+} for which weak intersystem transitions (oscillator strength $\sim 10^{-6}$) are expected to take place at $\sim 20\,000 \text{ cm}^{-1}$ and upwards, and Mn^{3+} for which a strong intrasystem transition (oscillator strength $\sim 10^{-3}$) is expected at $\sim 10\,000 \text{ cm}^{-1}$. The position and oscillator strength of the single absorption band found in CdS:Mn is better rationalized by Mn^{3+} . In this case only *one* intense absorption band, corresponding to the intrasystem transition is predicted,

$${}^5T_2 \rightarrow {}^5E = 10Dq, \quad (23)$$

which is followed at higher energies by weaker intersystem transitions. On the basis of this assignment we find for Mn^{3+} in CdS, $Dq = 780 \text{ cm}^{-1}$ (neglecting spin-orbit effects). The $|Dq|$ value for $\text{Mn}^{3+}(\text{H}_2\text{O})_6$ is reported as 2100 cm^{-1} by Holmes and McClure.⁸ Multiplying this quantity by the factor $4/9$ required by the tetrahedral coordination and reducing the result by $\sim 15\%$, in analogy with the case of Co^{2+} in going from ZnO to CdS, we obtain $Dq(\text{CdS}:\text{Mn}^{3+}) = 795 \text{ cm}^{-1}$, in quite good agreement with the value 780 cm^{-1} deduced from the observed absorption. The fact that spectra were observed only for Mn^{3+} does not, of course, eliminate the simultaneous presence of Mn^{2+} . Therefore, these results do not necessarily conflict with the electron spin resonance investigations of Lamb and Kikuchi,² and Dorain.¹

VIII. CdS:Cr

Although the positions of the various absorption bands are similar for various samples of CdS:Cr studied, the relative intensities vary quite markedly. Two representative samples will be discussed, numbers *I-72-3* and *I-79-2*. Spectrochemical analyses are reported for these samples in Table I. Chromium is the major impurity in both samples, and the percent of total sample weight is 0.0049% for sample *I-72-3*, and 0.022% for *I-79-2*; the latter sample also contains a comparable amount of Mn.

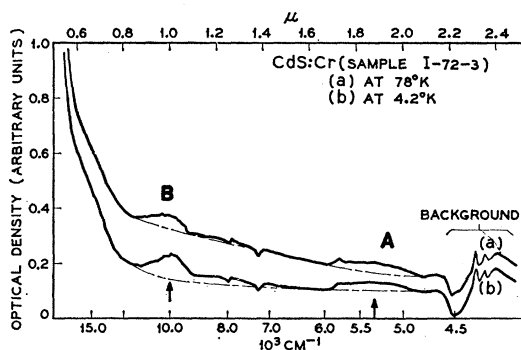


Fig. 18. CdS:Cr sample *I-72-3*, 1.51 mm thick. Absorption in 2.2- to 0.6- μ regions: (a) at 78°K ; (b) at 4.2°K .

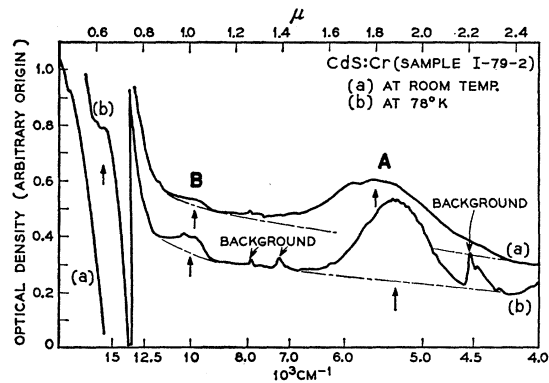


Fig. 19. CdS:Cr sample *I-79-2*, 0.83 mm thick. Absorption in 2.2- to 0.6- μ region: (a) at room temperature; (b) at 78°K . Compare with Fig. 18 and note differences in $\sim 5000 \text{ cm}^{-1}$ band in edge absorption.

The optical absorption in the 2.6- to 0.4- μ region shows a weak band at $10\,000 \text{ cm}^{-1}$ which is fairly similar in intensity and shape in both samples. Common also is an absorption roughly extending from 5000 to 6000 cm^{-1} , but in *I-72-3* it is quite flat and weak, while in *I-79-2* the absorption is bell-shaped, and fairly intense (Figs. 18 and 19). Also, the edge absorption for *I-79-2* is much steeper and has a shoulder at $15\,870 \text{ cm}^{-1}$ [Fig. 19(b)].

Since the absorption observed for Mn (Fig. 17) is not observed in the spectra of either of these samples, the Mn accidentally incorporated in *I-79-2* must be present as Mn^{2+} . As explained in the previous section, the lowest energy absorption for this ion in tetrahedral site symmetry in CdS should be in an energy range where it would be masked by the intense edge absorption. The differences in the spectra of the two samples are therefore to be ascribed to the chromium content and its ionic charge. It is conceivable that some limiting concentration is reached, near that of sample *I-72-3*, beyond which further introduction of Cr involves a different ionic state. The energy level schemes to be expected for the two most likely ionic states of chromium (Cr^{2+} and Cr^{3+}) in tetrahedral coordination are compared in Fig. 20 with the observed levels.

Since no crystal field parameters are known for Cr^{2+} and Cr^{3+} in tetrahedral coordination these parameters were estimated from values given by Tanabe and Sugano¹⁷ for $\text{Cr}(\text{H}_2\text{O})_6^{3+}$, namely $|Dq| = 1720 \text{ cm}^{-1}$ and $B = 765 \text{ cm}^{-1}$. For tetrahedral coordination Dq should be smaller than that given for the octahedral case by a factor of $4/9$; on the basis of the trend observed for B and Dq for Co^{2+} in different systems, coordination by sulfide ions will reduce these values by about 15% . We choose then

$$|Dq| = 700 \text{ cm}^{-1}, \quad B = 650 \text{ cm}^{-1}, \quad \text{and} \quad C = 4.5 B, \quad (24)$$

for Cr^{3+} in CdS. Similarly for Cr^{2+} ,

$$Dq = 560 \text{ cm}^{-1}, \quad B = 700 \text{ cm}^{-1}, \quad \text{and} \quad C = 4.8 B. \quad (25)$$

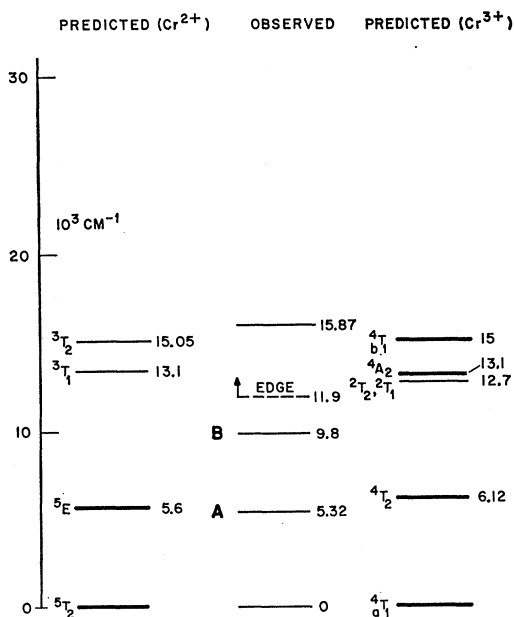


FIG. 20. CdS:Cr. Left: Predicted position of lowest cubic field terms for Cr²⁺ in tetrahedral coordination, assuming $|Dq| = 560$ cm⁻¹; $B = 700$ cm⁻¹; and $C = 4.8 B$. Right: Predicted position of lowest cubic field terms for Cr³⁺ in tetrahedral coordination, assuming $|Dq| = 700$ cm⁻¹; $B = 650$ cm⁻¹; and $C = 4.5 B$. Center: Observed positions of absorptions in CdS:Cr. (I-79-3).

It is apparent that, aside from the lowest excited term, the predicted positions of the various cubic symmetry terms do not agree very well with the observed spectra. However, if Cr³⁺ is present in appreciable concentration, then one should observe strong absorptions corresponding to the intrasystem transitions between 10 000 cm⁻¹ and 20 000 cm⁻¹ (Fig. 20, right). Although the shoulders on the edge absorption of sample I-79-2 occur in the energy range expected for these intrasystem transitions (Fig. 19), it is difficult to estimate the oscillator strength for these absorptions. A preliminary study of ZnS:Cr, where the edge absorption is at higher energies and does not interfere in the region under consideration, shows that ZnS:Cr has essentially the same spectra as observed for CdS:Cr (sample I-92-2), and that there are no intense absorptions comparable to band A in sample I-79-2 in the region of 10 000 to 20 000 cm⁻¹. We therefore assign the intense band A of sample I-79-2 to the transition from the ground term ⁵T₂ to ⁵E in the Cr²⁺ ion; as the energy difference for this transition represents 10 Dq , we find the value of Dq for Cr²⁺ in the tetrahedral coordination of CdS to be 530 cm⁻¹, in good agreement with the value we estimated *a priori*. Since the relative intensities of bands A and B differ for the two samples of CdS:Cr, band B may arise from a different ionic species than band A; perhaps B represents one of the intrasystem transitions for Cr³⁺. It is interesting to note that the intensity of band B is almost the same in both samples, although the Cr concentration differs by a factor of 5.

IX. CdS:V

A single characteristic spectrum was observed for the various samples of CdS doped with vanadium, although some samples also contained large quantities of copper and manganese. Copper was diffused simultaneously with the vanadium in an attempt to facilitate the introduction of the vanadium, while the manganese was introduced accidentally. Later experiments showed that vanadium could be introduced in comparable amounts into the CdS lattice without the assistance of Cu, by diffusing at higher temperatures (around 1200°C). The details of the spectra of one of the samples I-67-5, nominally doped with both Cu and V, are presented below; it should be emphasized that the spectrum of this sample is identical, except for over-all intensity of absorption, with the spectra of crystals containing vanadium impurities alone. The spectrochemical analysis summarized in Table I gives the following major impurity content: Cu, 0.11%; V, 0.0053%; Mn, 0.023%.

At room temperature the absorption spectrum consists of a triply peaked band of medium intensity (band A), centered at 8900 cm⁻¹, and of a broad structure (band B) superposed on the steeply rising edge absorption of the CdS matrix (Fig. 21). Cooling at 78°K and to 4.2°K serves only to increase the intensity of band A, and to sharpen the structure in the edge. A comparison with the spectra obtained for CdS:Mn (Fig. 17) and CdS:Cu (Figs. 1 and 2) shows that none of the observed absorptions in I-67-5 can be attributed directly to Mn³⁺ or Cu²⁺. This, of course, is to be expected, since, as mentioned above, samples doped with vanadium in which Cu and Mn are present in negligible quantities provide the same spectra as I-67-5.

As with chromium, no data are available for the crystal field parameters Dq , B , and C , for either V²⁺ or V³⁺ in tetrahedral coordination, and we are forced again to turn to the hexa-aquo complexes for an estimate of reasonable values. By decreasing $|Dq|$ to 4/9 of its value for octahedral coordination, and subsequently decreasing both Dq and B by 15% as we did for Cr and Mn, we obtain the analogous tetrahedral parameters

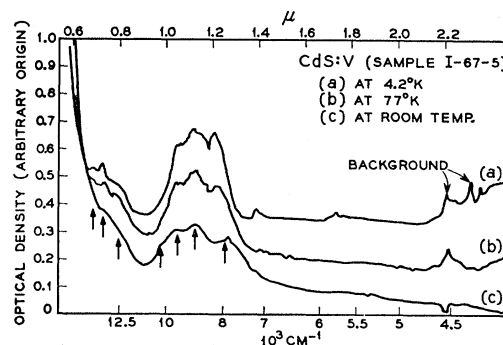


FIG. 21. CdS:V sample I-67-5, 1.54 mm thick. Absorption from 2.4 to 0.6 μ ; (a) at room temperature; (b) at 78°K; (c) at 4.2°K.

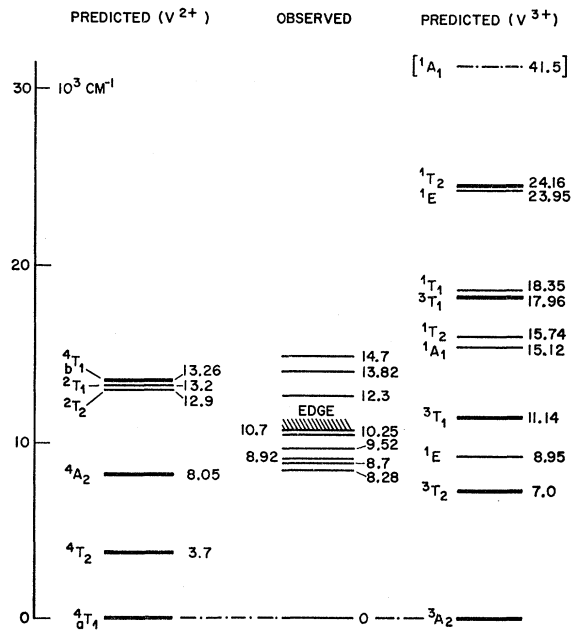


FIG. 22. CdS:V. Left: Predicted positions of lowest cubic field terms for V^{2+} in tetrahedral coordination, assuming $|Dq|=435$ cm^{-1} ; $B=680$ cm^{-1} ; and $C=4.6B$. Right: Same for V^{3+} , assuming $|Dq|=700$ cm^{-1} ; $B=540$ cm^{-1} ; and $C=4.5B$. Center: Positions of observed absorptions; the threshold of the edge absorption is also indicated.

for V^{2+} :

$$Dq=435 \text{ cm}^{-1}; B=680 \text{ cm}^{-1}; \text{ and } C=4.6B; \quad (26)$$

and for V^{3+} :

$$Dq=700 \text{ cm}^{-1}; B=540 \text{ cm}^{-1}; \text{ and } C=4.5B. \quad (27)$$

The energy levels resulting from the substitution of these values in the energy matrices of Tanabe and Sugano¹⁷ are shown in Fig. 22.⁴¹ Although the agreement of experiment with the spectra predicted for either ion is poor, the following considerations seem to exclude the possibility that the spectra arise from V^{2+} :

(a) The absorption ${}^4T_1 \rightarrow {}^4T_2$ predicted for V^{2+} at 3700 cm^{-1} is missing in the observed spectra.

(b) If the observed triply peaked band at 9500 cm^{-1} were to be identified with the transition to 4A_2 , according to the diagram for V^{2+} , then one would not expect any splitting of 4A_2 , either from noncubic components of the field or from spin-orbit coupling, contrary to observation.

(c) The transition ${}^4T_1 \rightarrow {}^4A_2$ is essentially a two-electron jump and as such should have a lower intensity than ${}^4T_1 \rightarrow {}^6T_1$ predicted at 13200 cm^{-1} , contrary to observation.

⁴¹ Exact energy level curves including spin-orbit coupling effects, but for different values of the B/C ratio, have been plotted by Liehr and Ballhausen.³⁶

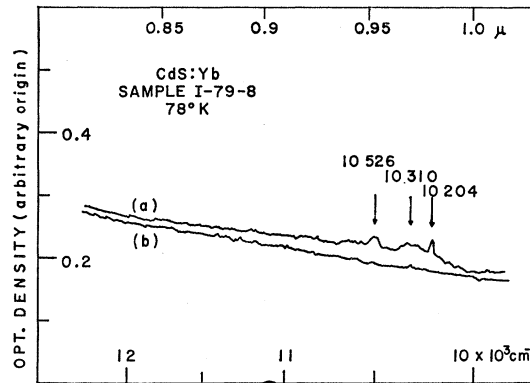


FIG. 23. (a) CdS:Yb sample I-79-8, 0.8 mm thick. Absorption at $78^\circ K$ in 10000 cm^{-1} region. (b) CdS:Dy at $78^\circ K$.

A comparison of the absorption spectra of CdS:V in Fig. 21 with the fluorescence excitation spectrum observed for the CdS:V phosphors reported in reference 5 shows that the two spectra are identical. However, the emission spectra in reference 4, for the same phosphors, cannot be correlated to the energy level scheme for the V^{3+} ion, but are in better agreement with what one might expect for V^{2+} .

X. CdS:Yb

The size of the Cd^{2+} ion is comparable to that of the rare-earth trivalent ions,¹⁸ so that trivalent rare-earth ions may also be introduced as substitutional impurities in CdS. Since the spectra of rare-earth ions are usually studied in coordination six, eight, or nine, it would be interesting to study the absorption spectra associated with tetrahedral coordination.

So far we have detected only weak absorptions arising from rare-earth ion impurities. Figure 23 shows the spectrum of CdS:Yb, sample I-79-8, at $78^\circ K$: the Yb spectrum is compared in the same figure with the spectrum of a dysprosium-doped CdS crystal, which does not absorb in the 10000 cm^{-1} region [Fig. 23(b)].

Three weak peaks are found at $78^\circ K$ in the spectrum of CdS:Yb, at 10204 cm^{-1} (sharp peak), 10310 cm^{-1} and 10560 cm^{-1} , which correspond to the transitions ${}^2F_{7/2} \rightarrow {}^2F_5$ for Yb^{3+} . A similar pattern of three peaks is found for ytterbium-doped yttrium gallium garnet crystals.²⁴

XI. CONCLUSIONS

It has been shown that the formalism of the crystal field theory can be applied successfully to interpret the absorption spectra of substitutional impurity ions of the first transition series in CdS. Generally speaking, the interpretation does not present serious difficulties for Cu^{2+} , Ni^{2+} , and Co^{2+} in CdS, because of the similarity of such spectra to the corresponding spectra in ZnO.

For the remaining ions of the series the agreement of the observed spectra with the predictions of the crystal field theory is still good, although some assignments

remain uncertain. These uncertainties are not really due to inadequacy of the crystal field approach, but rather stem from two reasons:

(a) Different ionic species (M^{2+} and M^{3+}) may be present together in the crystal.

(b) Only a very limited number of the absorption bands for some of the ions is available to check the consistency of the predictions with experimental data.

This latter inconvenience is due to the edge absorption which commences at low energies for CdS (and tends to be shifted to even lower energies in doped samples) thus obscuring crystal field absorptions over an extended region of the spectrum. The situation is more favorable in the case of ZnS where such edge absorption (even in doped samples) is located at higher energies.

Attempts to explain the *main* structure of individual bands using the simple model of cubic symmetry and spin-orbit coupling to first order have been successful only for isolated cubic symmetry terms. This approach is inadequate when the mixing of different cubic sym-

metry terms requires an extension of the spin-orbit treatment to higher orders, and when an explanation of the finer structure observed is required.

ACKNOWLEDGMENTS

The authors are greatly indebted to Dr. D. L. Wood for the use of the Cary spectrophotometer and low-temperature cryostat; to Dr. A. D. Liehr for valuable comments on the manuscript; to Mr. F. H. Doleiden for valuable technical assistance; and to Mr. E. R. Jaycox and Mr. D. L. Nash for performing the spectrochemical analysis of the samples.

APPENDIX

Wave functions for doublet terms of CdS:Co²⁺ (tetrahedral coordination) using the parameters $Dq=316$ cm⁻¹; $B=664$ cm⁻¹; $C=4.5 B$. The wave functions are expressed as linear combinations of states characterized by given subshell configuration and symmetry properties. $|{}^2T_2\rangle = \sum_j \alpha_j |d\epsilon^n(S_1\Gamma_1)d\gamma^{7-n}(S_2\Gamma_2), {}^2T_2\rangle$. The coefficients α_j are listed.

Term	Energy (10 ³ cm ⁻¹)	$d\epsilon^3({}^2T_2)d\gamma^4$	$d\epsilon^4({}^3T_1)d\gamma^3$	$d\epsilon^4({}^1T_2)d\gamma^3$	$d\epsilon^5d\gamma^2({}^1A_1)$	$d\epsilon^5d\gamma^2({}^1E)$
a_2T_2	15.45	-0.329	0.8171	0.0507	-0.2191	-0.416
i_2T_2	17.37	0.6707	0.3841	-0.4277	0.4632	-0.073
e_2T_2	21.36	-0.0882	0.3989	0.4303	0.3111	0.7423
d_2T_2	28.42	0.5767	-0.0066	0.744	-0.1865	-0.2810
c_2T_2	44.24	-0.3183	-0.1596	0.2751	0.7783	-0.4378
Term	Energy (10 ³ cm ⁻¹)	$d\epsilon^3({}^2T_1)d\gamma^4$	$d\epsilon^4({}^3T_1)d\gamma^3$	$d\epsilon^4({}^1T_2)d\gamma^3$	$d\epsilon^5d\gamma^2({}^3A_2)$	$d\epsilon^5d\gamma^2({}^1E)$
a_2T_1	13.47	0.892	-0.1615	0.344	0.1125	-0.2172
i_2T_1	17.41	-0.3761	-0.2075	0.8064	-0.3035	-0.2700
e_2T_1	19.58	0.0936	0.7129	0.4253	0.0390	0.5481
d_2T_1	20.44	-0.1578	-0.4480	0.2207	0.7571	0.3861
c_2T_1	29.38	0.1611	-0.4709	-0.0394	-0.5660	0.656
Term	Energy (10 ³ cm ⁻¹)	$d\epsilon^3({}^2E)d\gamma^4$	$d\epsilon^4({}^1A_1)d\gamma^3$	$d\epsilon^4({}^1E)d\gamma^3$	$d\epsilon^5d\gamma$	
a_2E	13.036	0.9427	-0.1953	-0.0453	0.2666	
i_2E	18.85	0.1804	0.3157	0.8961	-0.2542	
e_2E	23.204	-0.1628	0.3970	0.1457	0.8914	
d_2E	43.70					